AGU ADVANCING EARTH AND SPACE SCIENCES

Water Resources Research

RESEARCH ARTICLE
10.1029/2023WR035894

Baseflow Statistics in Aggregated Catchments

Mariaines Di Dato[1], Alberto Bellin[2], Vladimir Cvetkovic[3], Gedeon Dagan[4], Peter Dietrich[5,6], Aldo Fiori[7], Georg Teutsch[8], Alraune Zech[9], and Sabine Attinger[1,10]

[1]Department of Computational Hydrosystems, Helmholtz Centre for Environmental Research - UFZ, Leipzig, Germany, [2]Department of Civil, Environmental and Mechanical Engineering, University of Trento, Trento, Italy, [3]Department of Sustainable Development, Environmental Science and Engineering, Royal Institute of Technology (KTH), Stockholm, Sweden, [4]School of Mechanical Engineering, Tel Aviv University, Tel Aviv, Israel, [5]Department of Monitoring and Exploration Technologies, Helmholtz Centre for Environmental Research - UFZ, Leipzig, Germany, [6]Center of Applied Geoscience, University of Tubingen, Tubingen, Germany, [7]DICITA, Roma Tre University, Rome, Italy, [8]Helmholtz Centre for Environmental Research - UFZ, Leipzig, Germany, [9]Department of Earth Sciences, Faculty of Geosciences, Utrecht University, Utrecht, The Netherlands, [10]Institute of Environmental Science and Geography, University Potsdam, Potsdam-Golm, Germany

Key Points:

- Stochastic model to investigate the effect of temporal and spatial variability on the baseflow statistics in large heterogeneous catchments
- Baseflow statistics depend strongly on the ratio of recharge timescale and the geometric mean of reservoir timescales
- The temporal variance of baseflow is used to define an equivalent reservoir with its characteristic timescale

Correspondence to:
M. Di Dato,
mariaines.di-dato@ufz.de

Citation:
Di Dato, M., Bellin, A., Cvetkovic, V., Dagan, G., Dietrich, P., Fiori, A., et al. (2023). Baseflow statistics in aggregated catchments. *Water Resources Research*, *59*, e2023WR035894. https://doi.org/10.1029/2023WR035894

Received 22 JUL 2023
Accepted 22 NOV 2023

Abstract This paper employs stochastic analysis to investigate the combined effect of temporal and spatial variability on the temporal variance of baseflow in large catchments. The study makes use of the well-known aggregated reservoir model, representing the catchment as a network of parallel linear reservoirs. Each reservoir models a sub-catchment as an independent unit whose discharge temporal variation is characterized by a response time. By treating the rainfall-generated recharge and the sub-catchment response times as random variables, the statistical temporal moments of total baseflow are quantified. Comparisons are made between the temporal variance of baseflow in the aggregated reservoir model and that of a single homogeneous reservoir to define an upscaled response time. The analysis of the statistical moments of the random baseflow reveals that the number of reservoirs N has a weak impact on baseflow variance, with ergodic conditions achieved even with a small number of reservoirs. The study highlights that the ratio between the recharge correlation time and the geometric mean of the sub-catchment response times plays a critical role in baseflow damping and the upscaled response. The results indicate that the dynamics of baseflow generation depend not only on the catchment hydro-geological structure but also on the variability of the input signal. This research underscores the importance of understanding the combined influences of hydro-geological factors and recharge input variability for baseflow prediction under uncertainty. The present study should be regarded as a first step, setting the theoretical framework for future research toward incorporating field data.

1. Introduction

Groundwater discharge is a major contributor to streamflow in most rivers, especially in dry periods, which can potentially trigger drought conditions. The latter can be exacerbated by climate change, which manifests within the hydrological cycle with increasing frequencies and intensities of extreme events (Pörtner et al., 2022). This has raised the question about the capabilities of the groundwater reservoirs to mitigate the increasing (sub-)seasonal fluctuations and their impacts on ecosystems (Carlier et al., 2018). Hence, the overall characterization of aquifer systems with respect to their ability in sustaining river flow (baseflow) during prolonged drought periods becomes an increasingly relevant question even in moderate climates (Biswal & Marani, 2014; Fowler et al., 2022; Sutanto & Van Lanen, 2022). However, quantitative information on subsurface flow is generally sparse at regional scale (Gleeson et al., 2011, 2014). We can measure pressure head only at a few scattered observational wells and data on aquifer properties are limited to pumping test locations (Houben et al., 2022).

This paper presents a stochastic approach for modeling groundwater-fed baseflow. Using generally available rainfall data and river discharge data, baseflow characteristics are determined using stochastic tools to incorporate spatial heterogeneity and the associated uncertainty. This goes beyond the classical approach in hydrology, where baseflow response is interpreted by means of the hydraulic theory (e.g., Brutsaert, 1994; Brutsaert & Nieber, 1977; Troch et al., 2013) which typically neglects the heterogeneity of the aquifer properties within the catchment.

Input to the stochastic model is the groundwater recharge r, which is derived from rainfall data P, typically using a water balance approach (e.g., Healy, 2010). The statistical representation of the groundwater recharge time

series is achieved by modeling it as a stochastic process (e.g., Russian et al., 2013; Schuite et al., 2019). The latter is quantified by introducing a characteristic time scale λ, which, besides the inherent variability of the rainfall, is also impacted by the thickness of the unsaturated zone. If no other detailed information is available about the rainfall spatial distribution, groundwater recharge is assumed to be spatially homogeneous within each of the sub-catchments considered. Saturated flow is represented within each sub-catchment by a linear reservoir which is fed with time varying groundwater recharge derived from the water balance calculation and which, based on its effective properties, yields the recession or baseflow feeding the respective river reach. Approaches involving multiple linear reservoirs were already used by Moore (1997), who showed that parallel and serial linear reservoirs are able to model quite well a small catchment. Later, Clark et al. (2009) showed that a model composed of several linear reservoirs in parallel provided a consistent interpretation of experimental data in a mountain research watershed. Harman et al. (2009) developed a stochastic model on the basis of the conceptual model of Clark et al. (2009). They showed that non-linearity at the catchment scale can originate from heterogeneity in catchment characteristics. Later, Chen and Krajewski (2015) extended the work of Clark et al. (2009) and Harman et al. (2009) to large catchments and late-time recessions. Their results show that the recession parameters become less and less variable by increasing the catchment area.

In this paper we further explore the multiple linear reservoirs approach to baseflow, addressing several important issues like discussion of model conceptualization, the derivation of the statistical moments (mean and variance) as related to recharge and sub-catchments variability, and definition of an upscaled unique reservoir to model the system. Thus the two main objectives are: (a) to study the dynamics of baseflow, in particular how heterogeneously distributed reservoir timescales interplay with the temporal recharge variability to describe the temporal variance of the total baseflow and (b) to hypothesize an upscaling rule and the definition of equivalent parameters. To achieve these goals, the variance of the total baseflow is compared to the variance of a single (upscaled) linear reservoir to determine an equivalent parameter, which characterizes the catchment behavior. In our study, we apply the tools of stochastic analysis, which are well established in subsurface hydrology, to investigate the properties of heterogeneous hydrological catchments.

The conceptual model and the mathematical framework are detailed in the following sections, after which results are discussed and conclusions are drawn.

2. Theory

2.1. Catchment as a Natural Damper

A catchment responds to meteorological inputs by integrating several hydrological processes which act at various temporal and spatial scales. Among these hydrological processes, we focus here on the river baseflow Q, that is, the component generated from the shallow aquifers connected to the riverbed. The saturated groundwater reacts much slower to perturbations than surface or shallow unsaturated soil. As a consequence, the groundwater system buffers the temporal fluctuations of the recharge coming from the unsaturated zone, thereby acting as a natural damper. Hence, the temporal variance of baseflow σ_Q^2 is always smaller than the temporal variance of recharge σ_r^2 (see, e.g., Gelhar, 1974; Zhang & Schilling, 2004).

Such a dampening effect depends on the hydrogeological characteristics of the catchment. By using the tools of stochastic analysis, we seek to derive an analytical solution for the dampening of recharge fluctuations by a heterogeneous catchment. Applying such an analytical solution, we could infer the upscaled properties of the groundwater system if we know the baseflow and the recharge series, or the ratio of their temporal variances at least. The starting point is the conceptualization of the groundwater system within a river catchment, which is discussed in the following.

2.2. Catchment as Aggregated Linear Reservoirs

We consider a catchment feeding a river baseflow; such catchment can be divided in N sub-catchments, as conceptually displayed in Figure 1. Each sub-catchment $i (i = 1, \ldots, N)$ has an area A_i and contributes with the baseflow q_i to the river system of the catchment. The groundwater component of each sub-catchment is modeled as a linear reservoir governed by the linear ordinary differential equation

$$K_i \frac{dq_i(t)}{dt} = -q_i(t) + r(t), \tag{1}$$

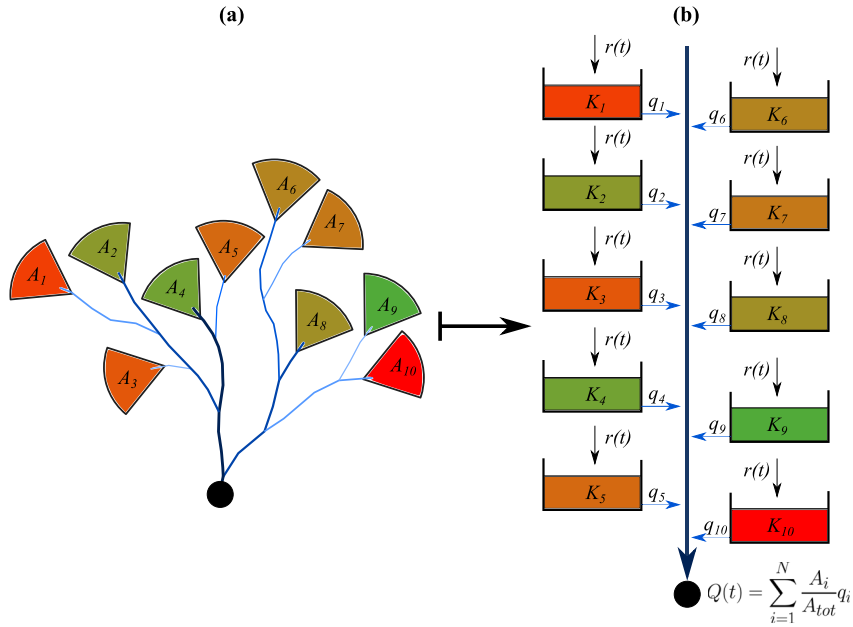

Figure 1. (a) Sketch of a catchment composed of $N = 10$ sub-catchments of areas $A_1, \ldots, A_{10}$. (b) Sub-catchments as linear reservoirs contributing the specific discharge q_i to the catchment specific discharge Q. K_i denotes the sub-catchment response time.

where $r(t)$ is the groundwater recharge which is assumed homogeneous throughout the catchment, for the sake of simplicity. K_i is the characteristic response time of sub-catchment i which lumps the impact of the sub-catchment's geological and spatial properties on the temporal response. For instance, in the case of rectangular sub-catchments $K = nL^2/(3T)$, with n the effective porosity, L the length of the sub-catchment and T its transmissivity (Gelhar, 1974). We remind that the linear reservoir is an approximate model for groundwater flow, derived from a linearized Boussinesq approximation of the flow equations (e.g., Fenicia et al., 2006; Haitjema, 1995; Vogel & Kroll, 1992). The solution of Equation 1 is given for the initial condition $q_i(t = 0) = q_{0,i}$ by

$$q_i(t) = q_{0,i} \exp\left(-\frac{t}{K_i}\right) + \int_0^t r(\tau) u(t - \tau; K_i) d\tau \tag{2}$$

where $u(t; K_i) = \exp(-t/K_i)/K_i$ is the transfer function for a linear reservoir model.

We define the total discharge Q as the sum of the N baseflow components q_i weighted by their fractional area $p_i = A_i/A_{tot}$, where $A_{tot} = \sum_{i=1}^{N} A_i$ is the total catchment area. Assuming that the travel time of water along the river network is small compared to the characteristic response times K_i of the individual groundwater sub-catchments (Zarlenga et al., 2022), the solution for $Q(t)$ then follows from the sum of the individual components given by Equation 2

$$Q(t) = \sum_{i=1}^{N} p_i q_i = \sum_{i=1}^{N} p_i \left(q_{0,i} \exp\left(-\frac{t}{K_i}\right) + \int_0^t r(\tau) u(t - \tau; K_i) d\tau \right) \tag{3}$$

Assuming stationary conditions, that is, $t \gg K_i$, we can neglect the impact of the initial conditions and the total baseflow results from

$$Q(t \gg K_i) = \sum_{i=1}^{N} p_i \int_0^t r(\tau) u(t - \tau; K_i) d\tau = \sum_{i=1}^{N} p_i \int_0^t \frac{r(\tau)}{K_i} \exp\left(-\frac{t - \tau}{K_i}\right) d\tau \tag{4}$$

The variables determining the total baseflow Q are the temporal variable recharge $r(t)$, that is, an external forcing assumed here to be spatially homogeneous, and the sub-catchments' characteristic response times K_i, which vary among sub-catchments.

2.3. The Stochastic Approach

2.3.1. Variability in External Forcing and System Properties

We apply a stochastic approach by modeling the recharge $r(t)$ as a random function and K_i as random variables which quantify the spatial variability of the system. In this manner, we merge the two approaches typically adopted in surface and subsurface hydrology. Specifically, surface hydrology focuses primarily on the variability of the external forcing ($r(t)$) while the catchment is considered almost homogeneous and acting as a filter. In contrast, hydrogeology prioritizes variability of hydraulic properties while external forcing is considered effectively constant. Our approach is a generalization where variability in both sub-systems, external forcing and hydraulic characteristics, are accounted for.

The variability in the external forcing is encapsulated in a temporally variable (but spatially constant) recharge $r(t)$. It is a time series which we model as a Random Time Function (RTF) fully characterized by its mean $\bar{r}$, its variance σ_r^2, both constant, and the following autocorrelation function $\rho_r(\tau) = \overline{\big(r(t+\tau)-\bar{r}\big)\big(r(t)-\bar{r}\big)}/\sigma_r^2$. Hereafter the overbar $\overline{(\dots)}$ indicates the ensemble average with respect to time.

This model is a reasonable approximation of groundwater recharge and takes into account the buffering effect of the unsaturated zone which reduces and possibly eliminates the intermittent character of the precipitations. Assuming that recharge is a continuous process not affected by intermittency is supported by field measurements (see, e.g., Majone et al., 2013; Russo et al., 2006).

The variability of the sub-catchment properties is modeled by regarding the response times K of the sub-catchments as random variables distributed according to the probability density function $f_K(K)$. As a first approximation we consider only the variability at scales larger than the characteristic dimension of the sub-catchments, that is, a constant K is assumed for each sub-catchment (see, e.g., Szilagyi et al., 1998). For the sake of simplicity, we assume that K_i are uncorrelated. Such a hypothesis is supported by observing that the characteristic dimension of the sub-catchments is typically of the order of kilometers while the integral scale of the transmissivity, which determines K, is generally smaller (see, e.g., Rubin, 2003, Table 2.1). In addition, we assume that r and K are also uncorrelated.

Given the above assumptions, the water flux Q at the control section of the catchment outlet, described by Equation 4, is a random time-dependent function whose statistical properties can be derived from those of K and r.

2.3.2. Variances of the Total Baseflow

A quantification of the base flow Q is provided by its first two moments, the mean and the variance. The moments with respect to the recharge describe the variability of Q induced by the temporal variability and uncertainty characterizing the external forcing simulated as an RTF, while the effect of the spatial variability of the hydraulic properties of sub-catchments can be quantified by averaging with respect to the random K. Notice that here we indicate the ensemble average with respect to time with an overbar $\overline{(\dots)}$ and the ensemble average with respect to space with brackets $\langle(\dots)\rangle$. In such a way, we aim to unify both the effects of spatial variability and the uncertainty affecting its characterization (see e.g., Dagan, 1989; Gelhar, 1993; Rubin, 2003).

We emphasize that the aggregated reservoirs model can in principle produce any type of residence time distribution, from unimodal to multimodal, in each single realization of the K field for the large $N \gg 1$ assumed here. In other words, multimodal distributions are also possible within realizations; an important basis for assuming alternative distributions is the variance of Q computed in this work.

The mean of Q is obtained by averaging with respect to both r and K in Equation 4, for $t \gg K_i$, $i = 1, \dots, N$

$$\langle \overline{Q} \rangle = \int dK \int dr\, Q(t) f_{r,K}(r,K) = \int dK \int dr\, Q(t) f_r(r) f_K(K) = \bar{r}, \tag{5}$$

where the assumption that r and K are independent allowed to write the joint pdf $f_{r,K}(r,K)$ of the two random functions as the product of their marginal pdfs: $f_{r,K}(r,K) = f_r(r) f_K(K)$. Hereafter our interest is in the system dynamics for sufficiently large times to eliminate the influence of the initial condition. Consequently, the conditional mean of Q with respect to r is $\overline{Q} = \int dr\, Q(t)\, f_r(r) = \bar{r}$ and the averaged discharge is independent of the distribution of K, whereby the ensemble mean with respect to K is immaterial. The fact that the mean base flow is equal to that of the recharge for a sufficiently large time reflects the mass conservation prevailing in the system.

It is convenient to differentiate the symbols for the variance with respect to time, due to the dependence on r, and the variance with respect to space, stemming from the dependence on K, in the same way as previously done for the mean. Hereinafter we indicate with σ_Q^2 and s_Q^2 the variance of the total discharge with respect to time and to space, respectively. The "total variance," that is, with respect to both time and space, is indicated with Var[Q]. The variance of the streamflow signal is therefore given by

$$\mathrm{Var}[Q] = \int d\,r \int d\,K \left(Q(t) - \bar{r}\right)^2 f_r(r)\, f_K(K), \tag{6}$$

where the relationship $\langle \overline{Q} \rangle = \bar{r}$, valid for $t \gg K_i$, $i = 1, \ldots, N$, was implemented. The variability of $\overline{Q(t)}$ through independent realizations of K, characteristic of the early times behavior, vanishes at late time when the system reaches stationarity.

After replacing Equation 4 into Equation 6 the following expression of the global variance is obtained

$$\mathrm{Var}[Q] = \langle \sigma_Q^2 \rangle + \bar{r}^2 \sum_{i=1}^{N} p_i^2 \int_0^t \int_0^t \left(\left\langle u\left(\tau'; K_i\right) u\left(\tau''; K_i\right) \right\rangle - \left\langle u\left(\tau'; K_i\right) \right\rangle \left\langle u\left(\tau''; K_i\right) \right\rangle \right) d\,\tau'\, d\,\tau'' \tag{7}$$

where $\langle u(\tau'; K) \rangle = \int dK\, u(\tau'; K)\, f_K(K)$ and $\langle u(\tau'; K)\, u(\tau''; K) \rangle = \int dK\, u(\tau'; K)\, u(\tau''; K)\, f_K(K)$ and

$$\langle \sigma_Q^2 \rangle = \sigma_r^2 \sum_{i=1}^{N} \sum_{j=1}^{N} p_i\, p_j \int_0^t d\,\tau' \int_0^t d\,\tau'' \rho\left(|\tau' - \tau''|\right) \left\langle u\left(\tau'; K_i\right) u\left(\tau''; K_j\right) \right\rangle \tag{8}$$

is the ensemble average, with respect to the random K, of the variance conditional on r

$$\sigma_Q^2 = \sigma_r^2 \sum_{i=1}^{N} \sum_{j=1}^{N} p_i\, p_j \int_0^t d\,\tau' \int_0^t d\,\tau'' \rho\left(|\tau' - \tau''|\right) u\left(\tau'; K_i\right) u\left(\tau''; K_j\right) \tag{9}$$

The second term of Equation 7 tends to zero as $t \gg \max(K_i)$. Under these conditions

$$\mathrm{Var}[Q] = \langle \sigma_Q^2 \rangle \tag{10}$$

The details of the derivation of Equation 7 are provided in Appendix A. From a physical point of view Equation 10 applies because mass conservation imposes that $\overline{Q} = \bar{r}$ irrespective of the spatial distribution of K which is independent of r. Both are reasonable assumptions of the system behavior, with the requirement that the statistics are evaluated for $t \gg K$ when the effect of the initial condition diminishes.

The pdf $f_K(K)$ encapsulates the effects on baseflow of both the spatial variability of K and its uncertainty, with the latter vanishing as $N \to \infty$. When the number of sub-catchments N increases, the system becomes ergodic, a condition manifested by the condition $\sigma_Q^2 \to \langle \sigma_Q^2 \rangle$. This is depicted in Figure 2, which summarizes graphically the information provided by the variances of Equation 8 (indicated with the gray vertical line) and Equation 9 (indicated with the black vertical line), respectively. Ergodicity is achieved when the characteristic dimension of the catchment is much larger than the correlation length of the hydraulic properties controlling groundwater flow. Thus, there is a hierarchy of scales: the scale of the sub-catchments, which is assumed to be sufficiently large relative to the transmissivity integral scale such as to warrant a constant K for each sub-catchment, and the scale of the catchment, which for $N \gg 1$ is much larger than the one prevailing for the various sub-catchments within the system.

Furthermore, it should be remarked that the sub-catchments characteristic size cannot be chosen arbitrarily, for example, according to a priori defined N value, but it should be of the order of the spatial correlation length of the hydraulic properties. This is the natural consequence of the hypothesis that variability at smaller scales does not influence the storage capacity of the sub-catchment and thereby K can be safely assumed constant within it.

Figure 2 sketches the impact of the number of sub-catchments N on the discharge variances. Under pre-ergodic conditions, N is too small to sample the space of possible K-values. Consequently, the total discharge differs between realizations of the catchment and each realization has a different temporal variance σ_Q^2 (i.e., the variance conditional on r, only). This manifests in the rugged graph depicting the aggregated Q in Figure 2a. As N increases, the collection of sub-catchments covers a wider range of K-values and, although local K-values are

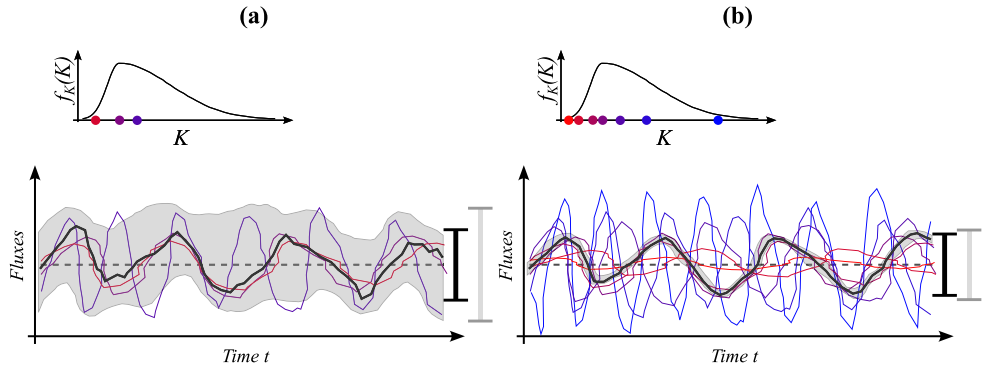

Figure 2. Sketching the impact of catchment size N on variability in average discharge Q: (a) under pre-ergodic and (b) quasi-ergodic conditions. The colors of sub-catchments reflect the value of K (blue—high, red—low) which is extracted form a skewed distribution $f_K(K)$. The dashed horizontal line indicates the mean recharge $\bar{r}$. The solid black line is the aggregated discharge Q and the shaded gray area is ensemble of all possible realizations. Vertical lines depict the amplitude of oscillation, namely the temporal variance. The black vertical line is the variance of the single realization σ_Q^2, while the gray vertical line is the variance of the ensemble, $\langle\sigma_Q^2\rangle$.

random, the aggregated Q of catchment realizations becomes close as manifested in the smoother graph of the aggregated Q of Figure 2b. As the difference between σ_Q^2 and $\langle\sigma_Q^2\rangle$ decreases, the mean discharge becomes deterministic. Thus $\mathrm{Var}[Q] \to \sigma_Q^2$ under ergodic conditions. The analysis of discharge variance reveals some similarity to that of dispersion for a contaminant traveling through a heterogeneous porous medium. Thus, the trajectory of the center of mass of a small plume relative to the velocity integral scale, is affected by large uncertainty as reflected by its time dependent variance. In contrast, for a large plume the center of mass moves with the mean velocity while the trajectories variance quantifies the rate of spreading of the actual plume around its center. Several authors for example, Kitanidis (1988), Dagan (1990, 1991), Andričević and Cvetković (1998), Attinger et al. (1999), and Dentz et al. (2000) published an extensive body of work on this topic in subsurface hydrology.

2.4. Effective Linear Reservoir and Equivalent Response Time

For upscaling, we seek to define a single reservoir model which displays the same behavior as the aggregated catchment model. We found that it is not possible to find an effective linear reservoir which has identical average behavior as the aggregated model, that is, sharing the same first two moments (mean, variance), as detailed in Appendix B. A system property is considered effective when it depends only on the statistics defining its spatial variability, as encapsulated by K, and not on the flow variability stemming from the recharge r. This is not applicable in our case because as shown in Appendix B it is possible to identify a single reservoir with the same variance σ_Q^2 of the catchment, but its value depends on the recharge statistics and, although in a weaker manner, on the number N of sub-catchments.

It is possible to define a linear reservoir whose discharge variance σ_{LR}^2 is identical to the temporal variance of the ensemble discharge $\langle\sigma_Q^2\rangle$. We define it as the *equivalent reservoir* and its characteristic timescale, the *equivalent characteristic timescale*, K_{eq}. Again, note that the equivalent linear reservoir does not completely reproduce the statistical behavior of the aggregated model (i.e., higher order moments), but only its temporal fluctuations around the ensemble discharge as quantified by the variance.

3. Illustrative Example

3.1. The Temporal Variance of the Total Baseflow

We present in the following section the results for the global variance (which coincides with the ensemble temporal variance), the temporal variance of the ensemble baseflow and the difference between these two variances, which vanishes under ergodic conditions.

To obtain numerical results, we assume the expression for the recharge autocovariance ρ_r, the timescale parameter distribution $f_K(K)$ and the fractional area p_i. Thus, the recharge autocovariance is selected as an exponential correlation function

$$\rho_r(\tau;\lambda) = \exp(-\tau/\lambda) \tag{11}$$

where λ is the recharge correlation time. The response times K_i are assumed to follow a log-normal distribution. We write K_i as $K_i = K_g \exp(y_i)$ where K_g is the geometric mean and y_i is a normally distributed variable with zero mean and variance s_y^2, that is, $y_i : \mathcal{N}\left[0, s_y^2\right]$ where $\mathcal{N}(y)$ denotes a normal distribution of y. Notice that we maintain the notation for the recharge variance σ^2 and the timescale variance s^2 because the former and the latter indicate variance with respect to time and space, respectively. For simplicity, we assume that the fractional area is the same for each reservoir, that is, $p_i = 1/\mathrm{N}$, such that the sum of the p_i is one and the sum of p_i^2 is given by

$$\sum_{i=1}^{N} p_i^2 = \frac{1}{N} \tag{12}$$

which vanishes for large N.

By substituting these expressions for ρ, K, and p_i into Equation 8, the following expression is obtained for the stream flow variance

$$\langle \sigma_Q^2 \rangle = \frac{\sigma_r^2}{N} \int \sigma_{LR}^2\left(\lambda';y\right)\mathcal{N}(y)\,dy + \frac{\sigma_r^2(N-1)}{N} \iint \frac{\exp(y_i)\sigma_{LR}^2(\lambda';y_i) + \exp(y_j)\sigma_{LR}^2(\lambda';y_j)}{\exp(y_i)+\exp(y_j)} \mathcal{N}(y_i)\mathcal{N}(y_j)\,dy_i\,dy_j \tag{13}$$

where $\lambda' = \lambda/K_g$ and

$$\sigma_{LR}^2\left(\lambda';y\right) = \frac{\lambda'}{\exp(y)+\lambda'} \tag{14}$$

is the baseflow temporal variance associated with a single linear reservoir with characteristic timescale equal to $K_g \exp(y)$ and unitary recharge variance (Gelhar, 1993, Chapter 3). The calculations of the variance for this specific case is detailed in Appendix C under transient conditions.

It is interesting to highlight the behavior of the total variance for the two extreme cases of $N = 1$ and $N \gg 1$. For $N = 1$, the temporal variance of the baseflow becomes:

$$\langle \sigma_Q^2 \rangle = \sigma_r^2 \int \sigma_{LR}^2\left(\lambda';y\right)\mathcal{N}(y)\,dy, \quad \text{for } N = 1 \tag{15}$$

which implies that for a catchment consisting of a single linear reservoir with uncertain timescale parameter, the expected temporal variance is the ensemble of the temporal variance of a single linear reservoir.

For $N \gg 1$ the system becomes ergodic, as previously discussed and the temporal variance of the aggregated baseflow becomes deterministic. The expression is the following:

$$\langle \sigma_Q^2 \rangle = \sigma_Q^2 = \sigma_r^2 \iint \frac{\exp(y_i)\sigma_{LR}^2(\lambda';y_i) + \exp(y_j)\sigma_{LR}^2(\lambda';y_j)}{\exp(y_i)+\exp(y_j)} \mathcal{N}(y_i)\mathcal{N}(y_j)\,dy_i\,dy_j, \quad \text{for } N \gg 1 \tag{16}$$

In Equation 16 one can recognize the weighted average of the linear reservoir variance for two generic reservoirs i and j. Due to the non-linearity of the variance operator, the aggregated variance is dependent on N though the system is linear.

We can also quantify the uncertainty of variance in non-ergodic conditions as the difference between the ensemble variance and the variance of a single realization, that is, $\langle \sigma_Q^2 \rangle - \sigma_Q^2$. Such a difference represents the amplitude of the shaded area in Figure 2 and decreases with the number of sub-catchments. We define this quantity as the *structural variance* s_Q^2, which is given by:

$$\begin{aligned} s_Q^2 &= \langle \sigma_Q^2 \rangle - \sigma_Q^2 \\ &= \frac{\sigma_r^2}{N}\left(\int \sigma_{LR}^2\left(\lambda';y\right)\mathcal{N}(y)\,dy - \iint \frac{\exp(y_i)\sigma_{LR}^2(\lambda';y_i) - \exp(y_j)\sigma_{LR}^2(\lambda';y_j)}{\exp(y_i)+\exp(y_j)} \mathcal{N}(y_i)\mathcal{N}(y_j)\,dy_i\,dy_j \right) \end{aligned} \tag{17}$$

The structural variance is indicated with the symbol s to highlight that it is a variance due to the uncertainty in the structural parameters K.

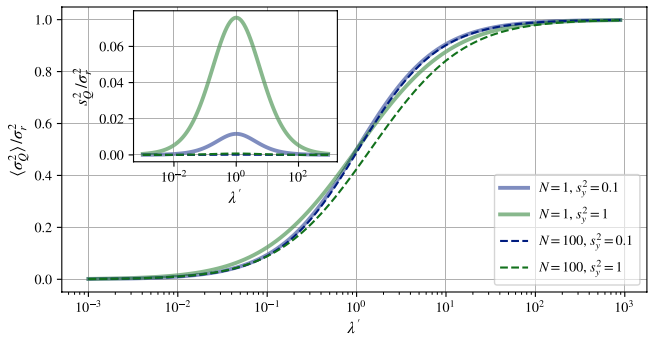

Figure 3. Total variance $\langle\sigma_Q^2\rangle$ with the inset showing the structural variance s_Q^2. Both quantities are plotted as a function of $\lambda' = \lambda/K_g$ for several values of N and s_y^2.

Figure 3 shows the total variance $\langle\sigma_Q^2\rangle$, with an inset depicting the behavior of the structural variance s_Q^2. It is reminded that both variables are normalized by the recharge variance σ_r^2 and are plotted as a function of the normalized correlation time of recharge λ'. The normalized global variance $\langle\sigma_Q^2\rangle/\sigma_r^2$ tends to zero for $\lambda' \ll 1$ and to one for $\lambda' \gg 1$. When heterogeneity is weak (as indicated by the blue lines), the aggregation associated with the magnitude of N plays a negligible effect and the solid ($N = 1$) and dashed lines ($N = 100$) overlap. In contrast, when the heterogeneity level is high ($s_y^2 = 1$, in green), σ_Q^2 decreases with N. Therefore, a heterogeneous catchment consisting of several hillslopes dampens the recharge fluctuations more than a homogeneous catchment with the geometric mean as a parameter.

As expected, the structural variance s_Q^2 increases with s_y^2 and decreases with N, thereby converging to zero for large N. This indicates that as N increases the uncertainty in the variance of Q vanishes and the baseflow becomes ergodic with respect to the heterogeneity in K. The structural variance has its maximum for $\lambda = K_g$ (i.e., $\lambda' = 1$), though quite small with regard to the recharge variance for the selected illustration, and tends to zero, independently of N or s_y^2, for $\lambda' \ll 1$ or $\lambda' \gg 1$. In fact, in such extreme cases (i.e., when K_g is much larger or much smaller than the recharge correlation time λ) the dampening is very large or very small and it does not depend on the heterogeneity of the system. For the same reason, also the total baseflow $\langle\sigma_Q^2\rangle$ is independent of the number of reservoirs N and heterogeneity level s_y^2 when $\lambda' \ll 1$ or $\lambda' \gg 1$.

Such behavior is confirmed by analyzing the variance of the total discharge under ergodic conditions (i.e., when $N \gg 1$), as shown by Figure 4. This variance is very much determined by λ'. For large λ' or recharge correlation times λ much larger than K_g, the temporal variance of the baseflow equals the temporal variance of the recharge and the aquifer transmits the incoming recharge signal almost unchanged. In contrast, for small λ' or recharge correlation times λ much smaller than K_g, the aquifer dampens the amplitude of the incoming recharge signal very efficiently and releases a baseflow signal with very small temporal fluctuations. The strength of the heterogeneity in K impacts the temporal variance of the total baseflow only for λ' in the range of $0.1 < \lambda' < 10$. The general rule is that a higher degree of variability in the K makes the temporal variance of the baseflow smaller. However, the comparison with the variance of a single linear reservoir (shown by circles) indicates that this effect is rather small for variance up to 0.5.

3.2. The Equivalent Response Time K_{eq}

As mentioned in Section 2.4, we seek to define an equivalent characteristic time K_{eq} by equating the temporal variance of the aggregated reservoirs and the temporal variance of a single linear reservoir. In order to obtain an analytical solution we assume that: (a) the catchment is under ergodic conditions, that is, $N \gg 1$ and (b) heterogeneity of the system is weak. Under such hypotheses, Equation 13 can be further simplified by expanding in a power series of y and taking the expectation. The approximations at the second order is given by

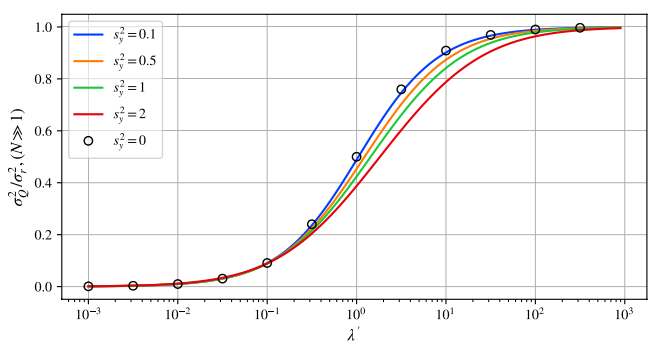

Figure 4. Total variance of baseflow in ergodic conditions ($N \gg 1$) as a function of λ' for several levels of heterogeneity. Black circles indicate the temporal variance for a single linear reservoir $\left(s_y^2 = 0\right)$.

$$\frac{\left\langle\sigma_Q^2\right\rangle^{(2)}}{\sigma_r^2} = \frac{\lambda'}{\lambda'+1} + \frac{\lambda'(1+\lambda'-2N\lambda')}{2N(1+\lambda')^3}s_y^2 \tag{18}$$

The ergodic limit ($N \gg 1$) is therefore given by

$$\frac{\sigma_Q^{2\,(2)}}{\sigma_r^2}(N \gg 1) = \frac{\lambda'}{\lambda'+1} - \frac{\lambda'^2}{(1+\lambda')^3}s_y^2 \tag{19}$$

We derive the equivalent characteristic time by equating Equation 19 with the expansion of the temporal variance for a single linear reservoir (i.e. Equation 14)

$$\frac{\sigma_{LR}^2}{\sigma_r^2} = \frac{1}{1+\kappa^*} \tag{20}$$

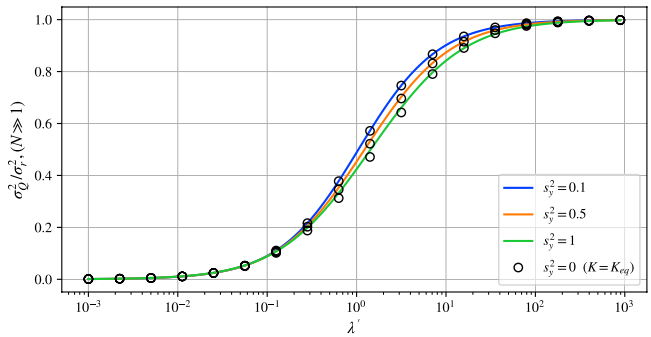

Figure 5. Comparison between the exact variance and the approximated variance. Solid lines indicate the exact solution and circles indicate the approximated solution for a linear reservoir with K_{eq} as characteristic parameter.

where $\kappa^* = K_{eq}/\lambda$ is a function of s_y^2. Therefore we can expand the equation with respect to s_y^2 up to the second order to obtain

$$\frac{\sigma_{LR}^2}{\sigma_r^2}^{(2)} = \frac{1}{1+\kappa^{*(0)}} - \frac{1}{\left(1+\kappa^{*(0)}\right)^2}\kappa^{*(1)}s_y^2 \tag{21}$$

where $\kappa^{*(0)} = K_g/\lambda = 1/\lambda'$ and $\kappa^{*(1)} = \partial\kappa^*/\partial\left(s_y^2\right)|_{s_y^2=0}$. By comparing Equation 19 with Equation 21, we obtain an identity for the first term, while for the second one we obtain:

$$\kappa^{*(1)} = \frac{1}{1+\lambda'} \tag{22}$$

The function κ^* is therefore given by

$$\kappa^* = \kappa^{*(0)} + \kappa^{*(1)}s_y^2 + O\left[\left(s_y^2\right)^2\right] = \frac{1}{\lambda'} + \frac{1}{1+\lambda'}s_y^2 + O\left[\left(s_y^2\right)^2\right] \tag{23}$$

By recalling that $\kappa^* = K_{eq}/\lambda$, K_{eq} is given by

$$K_{eq} = K_g\left(1 + \frac{\lambda'}{\lambda'+1}s_y^2\right) \tag{24}$$

It is clear that the upscaled characteristic time does not depend only on the catchment characteristics, that is, s_y^2, but also on the temporal characteristic of the input recharge. As a consequence, the upscaled behavior of an aggregated catchment can change according to a change in the correlation time of the input recharge.

Figure 5 shows the comparison between the exact variance at the ergodic limit for $N \gg 1$, depicted with a continuous solid line, and the variance of a single reservoir with $K = K_{eq}$, as given by Equation 24. The equivalent characteristic response K_{eq} gives an acceptable approximation for variances of K up to $s_y^2 = 1$. Moreover, such an upscaling rule is valid when λ and K_g have the same order of magnitude, given that only when λ' is close to unity heterogeneity influences the dampening of the recharge fluctuations.

4. Discussion

4.1. Assumptions and Limitations

Our results are based on an aggregated reservoir concept, which has been shown consistent with field data (see, e.g. Chen & Krajewski, 2015; Clark et al., 2009; Harman et al., 2009). The aggregated reservoirs model assumes that the recharge is homogeneous, the linear reservoirs are not correlated and that the routing time along the river network is negligible. Homogeneous recharge is assumed for simplicity but can be easily relaxed by assuming spatial correlation for recharge leading to a more complex analytical result. Similarily, we assume that $f(K)$ is unimodal and K_i are uncorrelated between sub-catchments. The latter assumption is geologically motivated given that the characteristic size of a sub-basin is typically larger than the length scale of hydraulic transmissivity, reported to be on the order of hundred meters (Rubin, 2003, Table 2.1). Furthermore, neglecting routing time along the river network implies neglecting its effect on the travel time distribution (Kirkby, 1976; Rinaldo & Rodriguez-Iturbe, 1996; Rinaldo et al., 1995). The effect of drainage networks has been investigated with a model composed of parallel hillslopes (Zarlenga et al., 2022). It was shown analytically that the lag time introduced by the river network is negligible or has a rather small effect on the discharge dynamics for very transmissive hillslopes. A similar behavior has been observed by Biswal and Marani (2010) who showed that the river network may have an impact only for steep catchments, which is equivalent to the assumption of large transmissivity in Zarlenga et al. (2022).

Despite its simplicity, the proposed framework is physically based as it relies on the linear reservoir model, which is equivalent to the Dupuit-Boussinesq aquifer at large times (Brutsaert & Nieber, 1977). By applying a stochastic framework to the aggregated reservoir model, we quantify the dampening effect by groundwater, employing only physically based parameters: the number of reservoirs N, the geometric mean K_g of the linear reservoir parameter K and its variance s_y^2. The number of reservoirs coincides with the number of sub-catchments in which the river

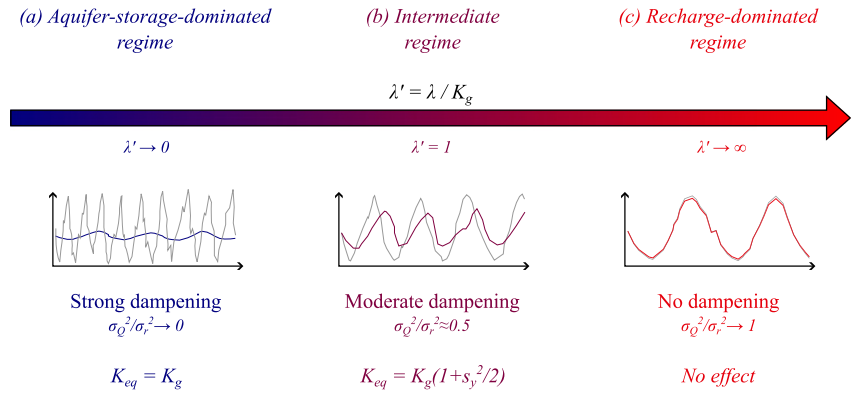

Figure 6. Different regimes associated with the value of λ': (a) Aquifer-storage-dominated regime; (b) Intermediate regime; and (c) Recharge-dominated regime. The gray curve represents the recharge variation with time, while the colored curves represent baseflow.

basin has been subdivided, and it depends on the resolution desired in the simulations. The mean of the reservoir parameters and their uncertainty can be quantified by analyzing discharge data. Brutsaert (2008) showed that the characteristic timescale (which can be compared to K_g in our modeling framework) stabilizes at about 1.5 months when increasing the catchment area, confirming ergodic behavior hypothesized in the present paper. Moreover, Brutsaert (2008) observed that the variability of K is relatively small, typically of the order of one or 2 weeks, thereby corroborating the low variability assumption that is the basis for an equivalent timescale calculation.

4.2. Implications

Recent developments in drought analysis have shown how the subsurface plays a leading role in mitigating drought propagation (de Matos Brandão Raposo et al., 2023). Therefore, understanding how groundwater resources can dampen the fluctuations of precipitation-generated recharge is key to quantifying drought development and recovery throughout the phases of the water cycle. The main result of the study can be grasped by distinguishing three dominant flow regimes depending on the ratio λ', as illustrated in Figure 6. In Figure 6a, the recharge time scale λ is much smaller than the characteristic mean residence time of the reservoir, as represented by K_g. In such a case, the aquifer storage affects significantly the baseflow fluctuations. The system dampens significantly the recharge and the baseflow variance σ_Q^2 is much smaller than the recharge variance σ_r^2, with their ratio tending in the limit toward zero. The variability of the sub-catchments response time K_i ($i = 1, \ldots, N$) manifests in the presence of different recession curves as shown in Figure 2a, which at system scale, by superposition, leads to an effective K_{eq} which is equal to the geometric mean of K_i of the sub-units. At the other extreme (Figure 6c), λ is much larger than K_g and recharge fluctuations dominate the baseflow behavior. As a consequence, the system baseflow variance σ_Q^2 is close to the recharge variance σ_r^2, with their ratio tending to one. This means that the recharge signal is only slightly dampened when passing through the subsurface aquifer system. The heterogeneity of the different aquifer sub-systems has practically no effect on the overall system recession behavior. In Figure 6b we observe a moderate dampening which is controlled by both, the subsurface aquifer storage properties as well as the recharge signal variance. This regime occurs when the recharge time scale λ is of the order of K_g and the corresponding K_{eq} depends on the structural heterogeneity s_y^2.

With the current status of any given catchment as a starting point, climate change will presumably lead to enhanced seasonality of rainfall and recharge, that is, more extensive rain periods during the winter and longer drought periods during summer; such a trend would lead to a shift of λ' and correspondingly to a different damping effect that does not depend on the geohydrological structure of the catchment. The proposed framework can provide one set of quantitative tools for analyzing flow regime shifts throughout a series of catchments with different scales and properties.

5. Summary and Conclusions

The present study investigates the dependence of the temporal statistical moments of the baseline discharge Q of a catchment on that of the input recharge r, as affected by the sub-catchments response times K_i, ($i = 1, \ldots, N$).

Since the mean values are equal $\left(\langle \overline{Q} \rangle = \bar{r}\right)$, the focus is on the ratio σ_Q^2/σ_r^2, which is less than unity and encapsulates the damping effect of the system. It must be noted that the dampening effect reflects the capability of the groundwater to mitigate recharge fluctuations. Thus, it can be interpreted as a measure of the catchment resilience to prolonged droughts, shown here to depend on the hydrogeological properties of the watershed.

Although simplified, the aggregated reservoirs model is physically based and allows to quantify baseflow dampening by using a few catchment's properties, such as the number of sub-catchments N, and the mean and the variance of the reservoir timescales, K_g and s_y^2, respectively. We recall here that the reservoir timescale K reflects the groundwater response which depends on the hydrogeological properties of the shallow aquifers connected to the river.

A first conclusion is that the impact of the number of sub-catchments N is relatively weak, and that ergodic conditions valid for $N \gg 1$ are reached even for a relatively small number N. Under ergodic conditions the damping factor σ_Q^2/σ_r^2 depends primarily upon $\lambda' \equiv \lambda/K_g$, the ratio between the time scale of the recharge λ and the geometric mean of the sub-catchments response times K_g. High damping occurs for $\lambda' \ll 1$, while there is practically no damping for $\lambda' \gg 1$. The damping factor grows monotonously between these limits and the main result of the study is quantifying its dependence upon arbitrary λ', as affected by the variance of the sub-catchments response time (Figure 5). As a practical consequence, by relating the damping effect to physically meaningful parameters (mean and variance of the response times), it would be possible to identify those watersheds that are more sensitive to prolonged or very severe droughts.

Another way to characterize the system behavior is to derive K_{eq}, the response time of a unique sub-catchment, which leads to the same damping as that of the sub-catchments ensemble. Similar to the damping factor σ_Q^2/σ_r^2, K_{eq}/K_g grows with λ'. As a consequence, an effective value that depends only on the geohydrological structure (encapsulated by K_i) and is independent of the recharge, cannot be defined. Under the assumption of weak heterogeneity corroborated by observations (Brutsaert, 2008), we derived an analytical solution for the equivalent reservoir response as a function of the ratio λ'. The dependence on the input recharge suggests that a catchment can change its equivalent behavior according to a change in the recharge, typically due to a change in precipitation regime. When the correlation time of recharge is smaller than the mean characteristic response, the baseflow fluctuations are influenced by the aquifer properties, leading to a very attenuated amplitude. In contrast, when the correlation time is much larger than the mean characteristic response, the baseflow fluctuations are dominated by recharge fluctuations and the resulting base flow is not damped. As a consequence, a change in the precipitation behavior might modify significantly the way a catchment can mitigate recharge fluctuations.

The present work aimed at developing a new theoretical framework for heterogeneous catchments, and for this reason we kept is as simple as possible by retaining only those processes we consider most relevant: the time variability of the recharge and the spatial variability of the groundwater storage effect, quantified by the variable K, which is modeled as random. The next envisaged step is validation with field data and comparison with distributed 3-D numerical models with the aid of a well monitored catchment. In particular, the numerical models, calibrated over a relatively wide geographical region, shall help in elucidating the leading hydrological processes at the catchment scale and test the validity of the conceptualizations adopted in the proposed framework.

Appendix A: Calculation of the Temporal Variance of Q

The temporal fluctuations of the total discharge Q with its statistical-averaged temporal-mean $\overline{\langle Q \rangle}$ is given by:

$$Q'(t) = Q - \overline{\langle Q \rangle} = \sum_{i=1}^{N} p_i \left\{ \int_0^t r(t-\tau)\, u(\tau; K_i)\, d\,\tau - \bar{r} \int_0^t \langle u(\tau; K_i) \rangle d\,\tau \right\} \tag{A1}$$

The variance is therefore the expected value of the square of the fluctuation:

$$\begin{aligned} \mathrm{Var}[Q] = \overline{\langle Q'(t)^2 \rangle} = \sum_{i=1}^{N}\sum_{j=1}^{N} p_i\, p_j \int_0^t d\,\tau' \int_0^t d\,\tau'' \\ \overline{\left\langle \left[r(t-\tau')\, u(\tau'; K_i) - \bar{r}\langle u(\tau'; K_i)\rangle \right] \left[r(t-\tau'')\, u(\tau''; K_j) - \bar{r}\langle u(\tau''; K_j)\rangle \right] \right\rangle} = \\ = \sum_{i=1}^{N}\sum_{j=1}^{N} p_i\, p_j \int_0^t d\,\tau' \int_0^t d\,\tau'' \left\{ \overline{r(t-\tau')\, r(t-\tau'')} \langle u(\tau'; K_i)\, u(\tau''; K_j)\rangle - \bar{r}^2 \langle u(\tau'; K_i)\rangle \langle u(\tau''; K_j)\rangle \right\} \end{aligned} \tag{A2}$$

Given that $\overline{r(t-\tau')\,r(t-\tau'')} = \sigma_r^2 \rho_r(|\tau' - \tau''|) + \bar{r}^2$, the final variance is:

$$\mathrm{Var}[Q] = \sum_{i=1}^{N}\sum_{j=1}^{N} p_i\, p_j \int_0^t d\,\tau' \int_0^t d\,\tau'' \left\{\sigma_r^2 \rho_r\left(|\tau' - \tau''|\right) \langle u(\tau'; K_i)\, u(\tau''; K_j)\rangle + \bar{r}^2\left[\langle u(\tau'; K_i)\, u(\tau''; K_j)\rangle - \langle u(\tau')\rangle \langle u(\tau'')\rangle\right]\right\} \tag{A3}$$

The sub-catchments are spatially uncorrelated, that is, $f(K_i, K_j) = f(K_i)\, f(K_j)$ for $i \neq j$, where f is the probability function of the response times K. Thus, the ensemble average $\langle u(\tau'; K_i)\, u(\tau''; K_j)\rangle$ for two reservoirs transforms as:

$$\begin{aligned}\langle u(\tau'; K_i)\, u(\tau''; K_j)\rangle &= \int dK_i \int dK_j\, u(\tau'; K_i)\, u(\tau''; K_j)\, f(K_i, K_j) \\ &= \int dK_i \int dK_j u(\tau'; K_i)\, u(\tau''; K_j)\, f(K_i)\, f(K_j) \\ &= \langle u(\tau'; K)\rangle\langle u(\tau''; K)\rangle \qquad \text{for } i \neq j \end{aligned} \tag{A4}$$

$$= \langle u(\tau'; K)\, u(\tau''; K)\rangle \qquad \text{for } i = j \tag{A5}$$

This expression is substituted in Equation A3 to further simplify the temporal variance in Equation 7.

Appendix B: Moment Analysis and Effective Linear Reservoir

Along a standard approach for linear systems, we analyze the temporal moments of the aggregated reservoir model. After Equation 4, the nth temporal moments of the discharge Q, of the recharge r and of the transfer function are defined as

$$Q_n = \frac{1}{\bar{r}} \int_0^\infty Q(t)\, t^n dt = \frac{1}{\bar{r}} \sum_{i=1}^{N} p_i \int_0^\infty t^n dt \int_0^t r(\tau) u(t-\tau; K_i) d\tau \tag{B1}$$

$$r_n = \frac{1}{\bar{r}} \int_0^\infty r(t)\, t^n dt \tag{B2}$$

$$U_{n,i} = \int_0^\infty u(t; K_i)\, t^n dt \tag{B3}$$

where $\bar{r} = \int_0^\infty r(t)\, dt$ is the total recharge volume (per unit area). After manipulation, we get for the first two moments

$$Q_1 = \sum_{i=1}^{N} p_i (r_1 + U_{1,i}) \tag{B4}$$

$$Q_2 = \sum_{i=1}^{N} p_i (r_2 + 2 r_1 U_{1,i} + U_{2,i}) \tag{B5}$$

$$S_Q^2 = Q_2 - Q_1^2 \tag{B6}$$

where S_Q^2 is the second-order temporal moment of Q. The above establishes a relation between the temporal moments of the quantities involved in Equation 4. Substituting $U_{1,i} = K_i$ and $U_{2,i} = 2K_i^2$ in the previous expressions and ensemble averaging over K_i, leads to

$$\langle Q_1\rangle = r_1 + \langle K\rangle \tag{B7}$$

$$\langle Q_2\rangle = r_2^2 + 2 r_1 \langle K\rangle + 2\langle K^2\rangle \tag{B8}$$

$$\langle S_q^2\rangle = \langle Q_2\rangle - \langle Q_1^2\rangle \tag{B9}$$

The term $\langle Q_1^2\rangle$ in Equation B9 is obtained by considering that the reservoirs i and j are not correlated when $i \neq j$

$$\langle Q_1^2 \rangle = \left\langle \sum_{i=1}^{N} \sum_{j=1}^{N} p_i p_j \left(r_1^2 + r_1 K_i + r_1 K_j + K_i K_j \right) \right\rangle \tag{B10}$$

$$= \left(r_1^2 + 2 r_1 \langle K \rangle + \langle K \rangle^2 \right) + \sum_{i=1}^{N} p_i^2 \left(\langle K^2 \rangle - \langle K \rangle^2 \right) \tag{B11}$$

Introducing the latter expression in Equation B9 leads to

$$\langle S_Q^2 \rangle = \sigma_r^2 + 2\langle K^2 \rangle - \langle K \rangle^2 - \sum_{i=1}^{N} p_i^2 \left(\langle K^2 \rangle - \langle K \rangle^2 \right) \tag{B12}$$

Introducing the lag-time $\Lambda = \langle q_1 \rangle - r_1$ and the dispersion $\Sigma = \langle S_q^2 \rangle - \sigma_R^2$, which corresponds to the mean and variance of the water travel time in the system (Rodríguez-Iturbe & Valdés, 1979), they are given by

$$\begin{aligned} \Lambda &= \langle K \rangle \\ \Sigma &= \langle K^2 \rangle + s_y^2 - \sum_{i=1}^{N} p_i^2 s_y^2 \end{aligned} \tag{B13}$$

It is seen that while the mean (lag-time) does not depend on the catchment size N, the variance (dispersion) does depend on it. The results for the limiting cases are:

- $N = 1$, that is, a small catchment (non-ergodic conditions): $\Sigma = \langle K^2 \rangle$
- $N \gg 1$, a large catchment (ergodic conditions): $\Sigma \simeq \langle K^2 \rangle + s_y^2$

Thus, the spreading caused by the aggregation of linear reservoirs increases with catchment size N, from $\langle K^2 \rangle$ to $\langle K^2 \rangle + s_y^2$.

Since the lag-time and dispersion pertaining to an effective single linear reservoir are equal to $\Lambda = K_{ef}$ and $\Sigma = K_{ef}^2$, with K_{ef} the effective reservoir constant, it is not possible to recover both moments Equation B13 of the aggregated catchments from a single reservoir with parameter K_{ef}.

Appendix C: Transient Solution for the Global Variance of Q for an Exponential ρ_r

Equation 9 can be solved by considering an exponential autocovariance $\rho_r(\tau) = \exp(-\tau/\lambda)$ and assuming that $K_i = K_g \exp(y)$, with y distributed as a normal function $\mathcal{N}$. The integral can be solved analytically by changing variables: $\tau' - \tau'' = z$ and $\tau' + \tau'' = \omega$:

$$\begin{aligned} \sigma_Q^2 = \sum_{i=1}^{N} \sum_{j=1}^{N} p_i\, p_j \int_0^t dz \int_z^{2t-z} d\omega\, \sigma_r^2 \exp\left[-\frac{z}{\lambda}\right] \left[u\left(t - \frac{\omega - z}{2}; K_g \exp(y_i)\right) u\left(t - \frac{\omega + z}{2}; K_g \exp(y_j)\right) + \right. \\ \left. u\left(t - \frac{\omega + z}{2}; K_g \exp(y_i)\right) u\left(t - \frac{\omega - z}{2}; K_g \exp(y_j)\right) \right] \end{aligned} \tag{C1}$$

which after integration leads to:

$$\begin{aligned} \sigma_Q^2(t) = \frac{\lambda' \sigma_r^2}{\exp(y_i) + \exp(y_j)} \left\{ \frac{\exp(y_i)}{\lambda' + \exp(y_i)} + \frac{\left[2\exp(y_i)\exp(y_j) - \lambda'(\exp(y_i) + \exp(y_j))\right] \exp\left[t\left(-\frac{K_g}{K_i} - \frac{K_g}{K_j}\right)\right]}{(\exp(y_i) - \lambda')(\lambda' - \exp(y_j))} - \right. \\ \frac{\lambda'(\exp(y_i) + \exp(y_j))\exp\left[-t\left(\frac{K_g}{\lambda} + \frac{K_g}{K_i}\right)\right]}{(\lambda' + \exp(y_i))(\lambda' - \exp(y_j))} \\ \left. - \frac{\lambda(\exp(y_i) + \exp(y_j))\exp\left[-t\left(\frac{K_g}{\lambda} + \frac{K_g}{K_j}\right)\right]}{(\lambda' - (\exp(y_i) + \exp(y_j)))(\lambda' + \exp(y_j))} + \frac{\exp(y_j)}{\lambda' + \exp(y_j)} \right\} \end{aligned} \tag{C2}$$

where $\lambda' = \lambda / K_g$. For $t \to \infty$, we obtain:

$$\sigma_Q^2 = \sum_{i=1}^{N}\sum_{j=1}^{N} p_i\, p_j\, \frac{\lambda'\sigma_r^2}{\exp(y_i)+\exp(y_j)}\left(\frac{\exp(y_i)}{\lambda'+\exp(y_i)}+\frac{\exp(y_j)}{\lambda'+\exp(y_j)}\right) \tag{C3}$$

By assuming the independence of K, taking the ensemble mean and recognizing the variance for a single linear reservoir, that is, $\sigma_{LR}^2 = \lambda'/(\exp(y)+\lambda')$, the final result for the global variance is Equation 13.

Data Availability Statement

Data were not used, nor created for this research.

Acknowledgments
We would like to thank Peter Troch and the Associate Editor for their invaluable guidance and constructive feedback throughout the review process. We are also deeply appreciative of the efforts made by the two anonymous reviewers whose thoughtful critiques and suggestions greatly contributed to the enhancement of this work. Additionally, the first author extends gratitude to the Helmholtz Centre for Environmental Research (UFZ) for their generous financial support, which has been instrumental in facilitating this research. AB acknowledges the support of the project DICAM-EXC (Departments of Excellence 2023–2027, Grant L232/2016) funded by the Italian Ministry of Education, University and Research (MUR). Open Access funding enabled and organized by Projekt DEAL.

References

Andričević, R., & Cvetković, V. (1998). Relative dispersion for solute flux in aquifers. *Journal of Fluid Mechanics*, *361*, 145–174. https://doi.org/10.1017/S0022112098008751

Attinger, S., Dentz, M., Kinzelbach, H., & Kinzelbach, W. (1999). Temporal behaviour of a solute cloud in a chemically heterogeneous porous medium. *Journal of Fluid Mechanics*, *386*, 77–104. https://doi.org/10.1017/S0022112099004334

Biswal, B., & Marani, M. (2010). Geomorphological origin of recession curves. *Geophysical Research Letters*, *37*(24), L24403. https://doi.org/10.1029/2010GL045415

Biswal, B., & Marani, M. (2014). 'universal' recession curves and their geomorphological interpretation. *Advances in Water Resources*, *65*, 34–42. https://doi.org/10.1016/j.advwatres.2014.01.004

Brutsaert, W. (1994). The unit response of groundwater outflow from a hillslope. *Water Resources Research*, *30*(10), 2759–2763. https://doi.org/10.1029/94WR01396

Brutsaert, W. (2008). Long-term groundwater storage trends estimated from streamflow records: Climatic perspective. *Water Resources Research*, *44*(2), W02409. https://doi.org/10.1029/2007WR006518

Brutsaert, W., & Nieber, J. L. (1977). Regionalized drought flow hydrographs from a mature glaciated plateau. *Water Resources Research*, *13*(3), 637–643. https://doi.org/10.1029/WR013i003p00637

Carlier, C., Wirth, S. B., Cochand, F., Hunkeler, D., & Brunner, P. (2018). Geology controls streamflow dynamics. *Journal of Hydrology*, *566*, 756–769. https://doi.org/10.1016/j.jhydrol.2018.08.069

Chen, B., & Krajewski, W. F. (2015). Recession analysis across scales: The impact of both random and nonrandom spatial variability on aggregated hydrologic response. *Journal of Hydrology*, *523*, 97–106. https://doi.org/10.1016/j.jhydrol.2015.01.049

Clark, M. P., Rupp, D. E., Woods, R. A., Tromp-van Meerveld, H. J., Peters, N. E., & Freer, J. E. (2009). Consistency between hydrological models and field observations: Linking processes at the hillslope scale to hydrological responses at the watershed scale. *Hydrological Processes*, *23*(2), 311–319. https://doi.org/10.1002/hyp.7154

Dagan, G. (1989). *Flow and transport in porous formations*. Springer-Verlag GmbH & Co. KG.

Dagan, G. (1990). Transport in heterogeneous porous formations: Spatial moments, ergodicity, and effective dispersion. *Water Resources Research*, *26*(6), 1281–1290. https://doi.org/10.1029/WR026i006p01281

Dagan, G. (1991). Dispersion of a passive solute in non-ergodic transport by steady velocity fields in heterogeneous formations. *Journal of Fluid Mechanics*, *233*, 197–210. https://doi.org/10.1017/S0022112091000459

de Matos Brandão Raposo, V., Costa, V. A. F., & Rodrigues, A. F. (2023). A review of recent developments on drought characterization, propagation, and influential factors. *Science of the Total Environment*, *898*, 165550. https://doi.org/10.1016/j.scitotenv.2023.165550

Dentz, M., Kinzelbach, H., Attinger, S., & Kinzelbach, W. (2000). Temporal behavior of a solute cloud in a heterogeneous porous medium: 1. Point-like injection. *Water Resources Research*, *36*(12), 3591–3604. https://doi.org/10.1029/2000WR900162

Fenicia, F., Savenije, H. H. G., Matgen, P., & Pfister, L. (2006). Is the groundwater reservoir linear? Learning from data in hydrological modelling. *Hydrology and Earth System Sciences*, *10*(1), 139–150. https://doi.org/10.5194/hess-10-139-2006

Fowler, K., Peel, M., Saft, M., Nathan, R., Horne, A., Wilby, R., et al. (2022). Hydrological shifts threaten water resources. *Water Resources Research*, *58*(8), e2021WR031210. https://doi.org/10.1029/2021WR031210

Gelhar, L. W. (1974). Stochastic analysis of phreatic aquifers. *Water Resources Research*, *10*(3), 539–545. https://doi.org/10.1029/WR010i003p00539

Gelhar, L. W. (1993). *Stochastic subsurface hydrology* (Vol. 390). Prentice-Hall.

Gleeson, T., Moosdorf, N., Hartmann, J., & van Beek, L. P. H. (2014). A glimpse beneath Earth's surface: Global hydrogeology maps (GLHYMPS) of permeability and porosity. *Geophysical Research Letters*, *41*(11), 3891–3898. https://doi.org/10.1002/2014GL059856

Gleeson, T., Smith, L., Moosdorf, N., Hartmann, J., Dürr, H. H., Manning, A. H., et al. (2011). Mapping permeability over the surface of the Earth. *Geophysical Research Letters*, *38*(2), L02401. https://doi.org/10.1029/2010GL045565

Haitjema, H. (1995). On the residence time distribution in idealized groundwatersheds. *Journal of Hydrology*, *172*(1–4), 127–146. https://doi.org/10.1016/0022-1694(95)02732-5

Harman, C. J., Sivapalan, M., & Kumar, P. (2009). Power law catchment-scale recessions arising from heterogeneous linear small-scale dynamics. *Water Resources Research*, *45*(9), W09404. https://doi.org/10.1029/2008WR007392

Healy, R. W. (2010). *Estimating groundwater recharge*. Cambridge university press.

Houben, T., Pujades, E., Kalbacher, T., Dietrich, P., & Attinger, S. (2022). From dynamic groundwater level measurements to regional aquifer parameters— Assessing the power of spectral analysis. *Water Resources Research*, *58*(5), e2021WR031289. https://doi.org/10.1029/2021WR031289

Kirkby, M. J. (1976). Tests of the random network model, and its application to basin hydrology. *Earth Surface Processes*, *1*(3), 197–212. https://doi.org/10.1002/esp.3290010302

Kitanidis, P. K. (1988). Prediction by the method of moments of transport in a heterogeneous formation. *Journal of Hydrology*, *102*(1), 453–473. https://doi.org/10.1016/0022-1694(88)90111-4

Majone, B., Viani, F., Filippi, E., Bellin, A., Massa, A., Toller, G., et al. (2013). Wireless sensor network deployment for monitoring soil moisture dynamics at the field scale. *Procedia Environmental Sciences*, *19*, 426–435. https://doi.org/10.1016/j.proenv.2013.06.049

Moore, R. (1997). Storage-outflow modelling of streamflow recessions, with application to a shallow-soil forested catchment. *Journal of Hydrology*, *198*(1), 260–270. https://doi.org/10.1016/S0022-1694(96)03287-8

Pörtner, H.-O., Roberts, D. C., Adams, H., Adler, C., Aldunce, P., Ali, E., et al. (2022). *Climate change 2022: Impacts, adaptation and vulnerability*. IPCC Sixth Assessment Report.

Rinaldo, A., & Rodriguez-Iturbe, I. (1996). Geomorphological theory of the hydrological response. *Hydrological Processes*, *10*(6), 803–829. https://doi.org/10.1002/(SICI)1099-1085(199606)10:6⟨803::AID-HYP373⟩3.0.CO;2-N

Rinaldo, A., Vogel, G. K., Rigon, R., & Rodriguez-Iturbe, I. (1995). Can one gauge the shape of a basin? *Water Resources Research*, *31*(4), 1119–1127. https://doi.org/10.1029/94WR03290

Rodríguez-Iturbe, I., & Valdés, J. B. (1979). The geomorphologic structure of hydrologic response. *Water Resources Research*, *15*(6), 1409–1420. https://doi.org/10.1029/wr015i006p01409

Rubin, Y. (2003). *Applied stochastic hydrogeology*. Oxford University Press.

Russian, A., Dentz, M., Le Borgne, T., Carrera, J., & Jimenez-Martinez, J. (2013). Temporal scaling of groundwater discharge in dual and multi-continuum catchment models. *Water Resources Research*, *49*(12), 8552–8564. https://doi.org/10.1002/2013WR014255

Russo, D., Zaidel, J., Fiori, A., & Laufer, A. (2006). Numerical analysis of flow and transport from a multiple-source system in a partially saturated heterogeneous soil under cropped conditions. *Water Resources Research*, *42*(6), W06415. https://doi.org/10.1029/2006wr004923

Schuite, J., Flipo, N., Massei, N., Rivière, A., & Baratelli, F. (2019). Improving the spectral analysis of hydrological signals to efficiently constrain watershed properties. *Water Resources Research*, *55*(5), 4043–4065. https://doi.org/10.1029/2018WR024579

Sutanto, S. J., & Van Lanen, H. A. J. (2022). Catchment memory explains hydrological drought forecast performance. *Scientific Reports*, *12*(1), 1–11. https://doi.org/10.1038/s41598-022-06553-5

Szilagyi, J., Parlange, M. B., & Albertson, J. D. (1998). Recession flow analysis for aquifer parameter determination. *Water Resources Research*, *34*(7), 1851–1857. https://doi.org/10.1029/98WR01009

Troch, P. A., Berne, A., Bogaart, P., Harman, C., Hilberts, A. G. J., Lyon, S. W., et al. (2013). The importance of hydraulic groundwater theory in catchment hydrology: The legacy of Wilfried Brutsaert and Jean-Yves Parlange. *Water Resources Research*, *49*(9), 5099–5116. https://doi.org/10.1002/wrcr.20407

Vogel, R. M., & Kroll, C. N. (1992). Regional geohydrologic-geomorphic relationships for the estimation of low-flow statistics. *Water Resources Research*, *28*(9), 2451–2458. https://doi.org/10.1029/92WR01007

Zarlenga, A., Fiori, A., & Cvetkovic, V. (2022). On the interplay between hillslope and drainage network flow dynamics in the catchment travel time distribution. *Hydrological Processes*, *36*(3), e14530. https://doi.org/10.1002/hyp.14530

Zhang, Y.-K., & Schilling, K. (2004). Temporal scaling of hydraulic head and river base flow and its implication for groundwater recharge. *Water Resources Research*, *40*(3), W03504. https://doi.org/10.1029/2003WR002094